Polymer 50 (2009) 645–653

Contents lists available at ScienceDirect

Polymer

journal homepage: www.elsevier.com/locate/polymer

Effect of compatibilization on the deformation and breakup of drops in step-wise increasing shear flow

F. Abbassi-Sourki [a], Michel A. Huneault [b], M. Bousmina [a,c,*]

[a] Canada Research Chair on Polymer Physics and Nanomaterials, Department of Chemical Engineering, Laval University, Ste-Foy, Quebec G1K 7P4, Canada
[b] National Research Council Canada, Industrial Materials Institute, Boucherville, Québec J4B 6Y4, Canada
[c] Institute for Nanomaterials and Nanotechnology (INANOTECH), Hassan II Academy of Science and Technology, Rabat, Morocco

ARTICLE INFO

Article history:
Received 5 September 2008
Received in revised form
10 November 2008
Accepted 15 November 2008
Available online 27 November 2008

Keywords:
Compatibilization
Drop breakup
Drop deformation

ABSTRACT

Drop deformation and breakup were investigated in the presence of a block copolymer in step-wise simple shear flow using a home-made Couette cell connected to an Anton Paar MCR500 rheometer. Polyisobutylene (PIB) was used as the matrix, while five different molecular weights of polydimethylsiloxane (PDMS) were selected to provide drops with a relatively wide range of viscosity ratio. A block copolymer made of PDMS-PIB was used for interfacial modification of the drop-matrix system. The copolymer concentration was 2 wt% based on the drop phase. The experiments consisted in analyzing the drop shape and measuring the variation of the length to diameter ratio, L/D, both in steady state and in transient regimes till breakup. This allowed revising of the classical Grace curve that reports the variation of the critical capillary number for breakup as a function of viscosity ratio and providing also a new one for blends compatibilized with an interfacial active agent with a given molecular weight.

© 2008 Elsevier Ltd. All rights reserved.

1. Introduction

The deformation and breakup of a Newtonian drop immersed in an immiscible Newtonian matrix have been extensively investigated from both experimental and theoretical standpoints. The first important studies in the area were undertaken by Taylor [1,2] who carried out experiments on drop deformation and breakup both in extensional and shear flow and proposed the first comprehensive model for drop deformation under small strains. Taylor's analysis describes the drop deformation with two dimensionless parameters: the viscosity ratio p and the capillary number Ca defined as

$$p = \frac{\mu_d}{\mu_m} \tag{1}$$

$$Ca = \frac{\mu_m a \dot{\gamma}}{\sigma} \tag{2}$$

where μ_d and μ_m represent the viscosities of the drop and the matrix, respectively, a denotes the initial radius of the spherical drop, $\dot{\gamma}$ is the applied shear rate and σ stands for the constant interfacial tension between the drop and the matrix. Since Taylor's work, important experimental, theoretical and numerical simulations efforts were devoted to understand the drop behavior under both small and large strains and to assess the conditions of drop breakup under various flow geometries and conditions. The general main findings of such studies are: i) When the deformation is small, the initial spherical drop deforms in time and attains an equilibrium ellipsoidal shape with the major axis L oriented with an angle θ close to 45° with respect to the flow direction, ii) When the deformation is increased, the major axis increases, while the other minor axes decrease to preserve the volume and the angle θ becomes smaller than 45° and the deformed drop becomes more oriented in the direction of flow [3–11]. If the deformation is increased further, no steady shape is obtained and the drop undergoes instable shape before breaking up into smaller droplets. The deformation and breakup conditions depend also on the capillary number, the viscosity ratio and the nature of flow (shear, uniaxial or planar flow). For a given viscosity ratio, the drop breaks up when the capillary number, Ca, exceeds a certain critical capillary number, Ca_{crit} The variation of Ca_{crit} with the viscosity ratio was determined experimentally by Grace [12] for a single Newtonian drop suspended in a Newtonian medium in both shear and elongational flows. The experimental data of Grace can be fitted by the following empirical equation:

* Corresponding author. Institute for Nanomaterials and Nanotechnology (INANOTECH), Hassan II Academy of Science and Technology, Rabat, Morocco. 225, Av. MD Ben Hassam El Ouzzani, Quartier Ambassador, Souissi, Rabat. Tel.: +212 3775 0179; fax: +212 3775 8171.
E-mail address: m.bousmina@inanotech.ma (M. Bousmina).

0032-3861/$ – see front matter © 2008 Elsevier Ltd. All rights reserved.
doi:10.1016/j.polymer.2008.11.027

$$\log Ca_{crit} = -0.370 + 0.185(\log p)^2 + 0.0177(\log p)^3 - \frac{0.115}{\log p - \log 4.5} \quad (3)$$

The above empirical equation has similar form as the one proposed by De Bruijn [13] but we found that it gives slightly better fit of the experimental results particularly at low viscosity ratio than De Bruijn's equation. The variation of Ca with p for intermediate flows between elongational and shear flow was provided by Bentley and Leal [5]. The mechanism of deformation and breakup has been studied by various authors [3,14,15]. Depending on the ratio of Ca/Ca_{crit}, the drop will either deform or break. For $p < 1$ and $Ca/Ca_{crit} < 1$, the drop deforms and distorts, but it does not break; it breaks only when $Ca/Ca_{crit} > 1$. In this case it undergoes a sigmoidal shape before experiencing tip-streaming (fragmentation at the ends) that results in ejection of small droplets from the ends. For the case of $p \approx 1$ and $Ca/Ca_{crit} > 1$, the drop necks and breaks in the middle by generating two small daughter droplets with some satellite droplets in between aligned on the same axis and equally distanced from each other. For $Ca/Ca_{crit} \gg 1$, the drop deforms first into a long thread and then breaks through Rayleigh capillary instabilities [16].

When an interfacial active agent is added to the system, the mechanisms of deformation and breakup change substantially. The presence of such interfacial active agent decreases the interfacial tension, which leads to an increase in the capillary number and consequently a change in the drop deformation [17–21]. If the deformation is large, the interfacial active agent distribution along the surface becomes non-uniform, which leads to a non-uniform drop deformation. Clearly, in the presence of an interfacial active agent, the drop deformation is not only controlled by the viscosity ratio and the capillary number, but also by two additional parameters: i) the surface Peclet number, P_e and ii) the interfacial tension ratio, I_r. P_e is defined as the ratio between the surface convective flux, $J_C = \sigma\dot{\gamma}a$, that promotes the concentration gradient, and the surface diffusion flux, $J_D = D_S\sigma/a$, that tends to restore homogeneous concentration distribution of the interfacial active agent molecules along the drop surface:

$$P_e = \dot{\gamma}a^2/D_S \quad (4)$$

where σ is the interfacial tension under quiescent conditions and D_S is the surface diffusivity of the interfacial active agent molecules. I_r is given by

$$I_r = \sigma(x,t)/\sigma_0 \quad (5)$$

σ_0 is the interfacial tension in the absence of the interfacial active agent (clean surface) and $\sigma(x,t)$ is the interfacial tension in the presence of the interfacial active agent that changes in time along the drop surface. In turn, such spatial variation in the interfacial tension changes the capillary number that becomes

$$Ca^* = Ca_{crit}/(1-\beta) \quad (6)$$

where Ca_{crit} is the critical capillary number of clean drop and Ca^* is the critical capillary number in the case of interfacial active agent modified drop:

$$\beta = 1 - I_r \quad (7)$$

The change in the drop deformation is a consequence of an additional interfacial term that appears in the equation of the stress jump across the interface [22]:

$$[-P]\mathbf{n} + [\mathbf{n}\cdot\mathbf{T}] = -\frac{\partial\sigma}{\partial\Gamma}\nabla_s\Gamma + 2H\sigma\mathbf{n} \quad (8)$$

where P is the pressure, $\mathbf{T}$ is the stress tensor, $\mathbf{n}$ represents the outward pointing unit normal vector, σ denotes the interfacial tension, Γ is the surface concentration of the interfacial active agent and $2H$ stands for the mean curvature of the interface. The two terms in left-hand side are, respectively, the isotropic pressure ($[-P]$) and the stress jump at the interface ($[\mathbf{n}\cdot\mathbf{T}]$) and those of the right-hand side represent the tangential Marangoni stresses ($(\partial\sigma/\partial\Gamma)\nabla_s\Gamma$) and the curvature term ($2H\sigma$). Stone and Leal [22] and others [23–26] have shown that for high values of P_e, the interfacial active agent molecules are swept towards drop tips and thus lower the local interfacial tension. As a consequence of local interfacial tension lowering is an increase in the curvature term (tip-stretching) to ensure the stress balance. However, if the early concentration gradient of the surface active agent between the tips and the drop equator is high, the local concentration approaches the saturation and consequently, strong Marangoni stresses appear in the opposite direction. Such effect retards the convective flux and immobilizes the interface against deformation. At low P_e, the interfacial active agent concentration remains almost uniform over the entire interface. During deformation process, the local interfacial agent concentration may decrease due to the increase in the drop surface area. This results in an increase in the local interfacial tension that becomes larger than the initial equilibrium value, which reduces the drop deformation.

The aim of this work is to reconstruct the Grace curve for the case of interfacial active agent modified drops and at the same time examine the mechanism of their deformation before breakup. The experiments were conducted on a home-made and independently motor driven transparent visualization cell connected to a MCR500 Paar Physica rheometer.

2. Experiments

2.1. Materials

Table 1 reports all the polymers used in this study along with their source and some of their characteristics. The matrix was a polyisobutylene 920 (PIB920) and the drops were various grades of polydimethylsiloxane (PDMS) with different molecular weights. Fig. 1 shows the steady shear viscosity measured with an Anton Paar MCR500 rheometer at 24 °C using a 50 mm cone-plate geometry having a cone angle of 1.995°.

All polymers exhibit Newtonian behavior in the investigated shear rate range with a constant viscosity and zero first normal stress difference. High molecular weight polymers do show some traces of the first normal stress difference but only at high shear rates that are well above the maximum shear rate used in the work. PIB and PDMS are immiscible and transparent with different refractive indices at room temperature suitable for in situ morphological characterization. The interfacial modifier was a diblock copolymer of PIB–PDMS purchased from Polymer Source, Inc. with a weight average molecular weight of the PIB and PDMS blocks of 8400 g/mol

Table 1
Material characteristics at 24 °C.

Material	Molecular weight (M_w)[a]	Viscosity (Pa s)	Source
PDMS0.1	8200	0.1	Fluka Company
PDMS1	45,000	0.93	Sigma–Aldrich
PDMS10	76,000	10.65	Sigma–Aldrich
PDMS30	94,000	29.35	Sigma–Aldrich
PDMS60	121,000	60.15	Fluka Company
PIB920	1390	25.9	Sigma–Aldrich
Block copolymer	18,000[b] PIB block: 8400 PDMS block: 9600	6800[c]	Polymer source

[a] Measured.
[b] Supplied by the manufacturer.
[c] At 30 °C.

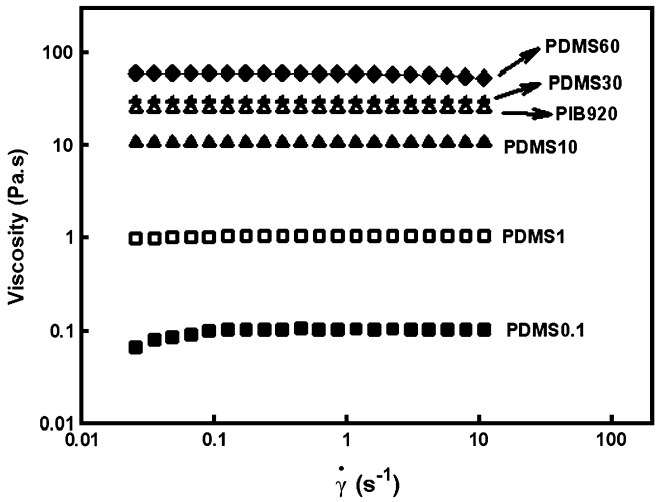

Fig. 1. Steady shear viscosity as a function of shear rate ($\dot{\gamma}$) for the various used polymers.

and 9600 g/mol, respectively. The polymolecularity index of both blocks was 1.2. PIB block has M_w larger than its critical molecular M_c (M_c: 5700 g/mol) [27], while M_w of the PDMS block is relatively smaller than its M_c (10,000 g/mol). The viscosity of the PIB was 26 Pa. s while that of the various PDMS varied from 0.1 to 60 Pa. s.

2.2. Flow visualization device

The visualization of the drop deformation and breakup during shearing was carried out with a home-made and patented Couette device with two coaxial cylinders rotating in opposite directions (see Fig. 2) [28]. The outer cylinder was made from quartz with high quality surface finish and high transparency. It is rotated separately by means of a servo-motor placed under the rheometer. The inner stainless steel cylinder is connected to the shaft of the Anton Paar MCR500 rheometer. Such configuration allows rotating separately each cylinder in any desired direction with the same or different velocities. In the present case, the two cylinders were rotated at the same speed in the opposite directions, which ensured having the drop fixed in space during shear, suitable for drop dynamics visualization. The system was assembled such that concentricity of the two cylinders was ensured.

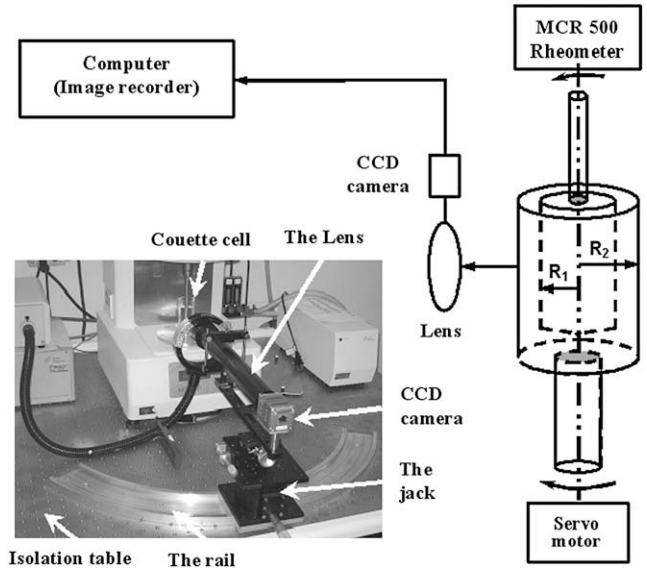

Fig. 2. Schematic and image of the home-made Couette device and the corresponding accessories used to record drop deformation and drop breakup images ($R_1 = 13.3405$ mm, $R_2 = 15.00$ mm).

The drop deformation was captured in time by means of a CCD Pixelfly camera. An ELWD Telecentric gauging lens was fixed to the camera and both of them were installed on a precision jack, which offered a movement along the three directions of space. The jack, the camera and the lens assembly were mounted on a circular aluminum rail allowing lateral movements of the camera while keeping the same focal distance with respect to deforming drop. The whole measurement and imaging assembly was mounted on an active self-leveling vibration isolation table, where the active-air leveling mechanism provided leveling compensation for any deflection of work station using three air servo valves in the legs linked to the underside of the table. This offered a constant working height during all measurements.

Interfacial tension of all samples was determined by the retraction method of a slightly deformed drop using a Linkam Scientific Instrument CSS450 mounted on an optical Axipsckop Zeiss microscope. After the slight deformation, the shear was canceled and the drop was let to relax and retract back to its spherical equilibrium shape. The interfacial tension was then determined from the variation of the drop dimensions in time [29].

2.3. Sample preparation

The liquid samples were prepared by mixing the diblock copolymer and the drop phase (PDMS) by means of a stirrer. The amount of the copolymer was kept constant at 2 wt% of the drop phase. In preparation to visualization experiments, the outer cylinder was first filled with the suspending medium (PIB920) and then the inner cylinder was lowered until its upper part was covered with 3 mm of the suspending liquid matrix. The PDMS drop was injected into PIB matrix by means of a syringe around the central part of the gap. Since in all experiments, the maximum drop size (60 μm) is much smaller than the gap (1.5 mm), wall effects can be considered as negligible. When the drop became quite stable in shape, a first picture was taken and used as a reference in the absence of flow.

2.4. Flow in a Couette cell

Assuming isothermal, laminar and steady shear flow under negligible gravity and end effects, the velocity profile $u_\theta(r)$ in the gap between the two cylinders is given by

$$u_\theta(r) = \frac{\Omega_2 R_2^2 - \Omega_1 R_1^2}{R_2^2 - R_1^2} r + \frac{(\Omega_1 - \Omega_2) R_1^2 R_2^2}{R_2^2 - R_1^2} \frac{1}{r} \tag{9}$$

where R_i and Ω_i ($i = 1, 2$) are the radius and the angular velocity of the inner and the outer cylinders, respectively, and r represents the radial position in the annular gap. Since the two cylinders counter-rotate, the angular velocities Ω_1 and Ω_2 have opposite signs. To capture the drop images by the CCD camera during deformation or breakup, the drop should always be kept in the camera viewing window without any circumferential movement, so its linear velocity, i.e. $u_\theta(r)$, would be 0 and thus the shear rate profile in the annular gap deduced from Eq. (9) is given by

$$\dot{\gamma}(r) = \frac{2\left(\Omega_2 R_2^2 - \Omega_1 R_1^2\right)}{R_2^2 - R_1^2} \tag{10}$$

Eq. (10) implies that there is no need to know the radial position of the drop in order to calculate the applied shear rate. Considering

the geometry of our system, $R_1 = 13.3405$ mm and $R_2 = 15.00$ mm and changing the angular velocity of cylinders, Ω, to revolution per minute, N, Eq. (10) leads to

$$\dot{\gamma} = 1.00N_2 + 0.793N_1 \quad (11)$$

where $\dot{\gamma}$ is the shear rate in s^{-1} and N_1 and N_2 are the rotation speeds in revolution per minute (rpm) of the inner and the outer cylinders, respectively.

3. Results and discussion

Table 2 lists the interfacial tension of various clean and compatibilized PDMS drops in PIB920 matrix. Within the experimental errors, all clean PDMS/PIB systems are characterized by interfacial tension values that are approximately in a same range, however, the lowest viscosity PDMS having the smallest M_w shows a lower interfacial tension. A possible explanation in this case is that the PDMS0.1 has a weight average molecular weight, M_w, smaller than the critical molecular weight for entanglements (10,000 g/mol). It may also be due to the possible migration of the shorter chain molecules towards the drop surface leading to lowering of the interfacial tension [30]. Similar observations have been reported [31–33].

Contrary to clean samples, the interfacial tensions for copolymer modified systems do not show a regular trend. Such scattering in interfacial tension values might be related to two factors. First, we have used Taylor's equation for drop relaxation that was derived for clean systems and second the distribution of the copolymer on the drop surface changes both during deformation and during relaxation of the drop. The use of deformed drop retraction method to estimate the interfacial tension of compatibilized drops was criticized by Velankar et al. [34]. They reported that this method underestimates interfacial tension values especially for viscosity ratios smaller than unity. In another method proposed by Hu [35] and also by Yu et al. [36], a second order drop deformation was used to determine the interfacial tension of block copolymer modified interfaces. The interfacial tension values obtained using Hu's second order method are also listed in Table 2.

3.1. Deformation and breakup shear rate

The first series of deformation experiments consisted in examining the steady state deformation for clean and compatibilized drops at different shear rates for various viscosity ratios. The initial shear rate was selected to be lower than the critical shear rate of breakup ($\dot{\gamma} \ll \dot{\gamma}_{crit}$). When the drop attained its steady deformed shape, the shear rate was then gradually incremented and for each increment the drop was allowed to reach its new steady deformed shape. The procedure was continued until the breakup occurred. The results of such experiments for various viscosity ratios are reported in Fig. 4a–e that present the steady state L/D as a function of the velocity gradient across the drop ($\dot{\gamma}a$), where L is the projection of the major axis on the vorticity–shear plane and D is the initial drop diameter ($D = 2a$). Since the true major axis of the deformed drop (L') has a tilt angle θ with the surface plane (see Fig. 3), only the projection of L' (L) on the plane perpendicular to the velocity gradient is measured [37]:

$$L = 2\sqrt{L'^2\cos^2\theta + B'^2\sin^2\theta} \quad (12)$$

The L/D ratio of uncompatibilized drops increases slowly with the velocity gradient up to a critical value at which the drop breaks up. Each point on the figure corresponds to steady sate deformation at the given shear rate and the last recorded data point corresponds to last shear rate at which no steady state deformation is obtained resulting in a continuous deformation followed by breakup.

The drops comprising PDMS–PIB copolymer show a much larger deformation than their non-compatibilized counterparts. For the lowest viscosity ratio, $p = 0.0039$, presented in Fig. 4a, the compatibilized drop shows an unusual behavior. The L/D ratio increases rapidly in the initial stage due to extending the drop tips. The end portion of the drop tips then disintegrates from the main drop to very small droplets causing a reduction in L/D. Applying higher shear rates does not greatly affect the drop tip-to-tip length resulting in pseudo-stabilization of the L/D of the drop (smooth increase). The drop keeps this behavior until its L/D drops to lower value at about 0.0045 cm/s before increasing again. In this case, the breakup critical shear rate for the copolymer modified drop is the same as for the clean drop. This behavior will be discussed later when examining the drop images.

For the higher viscosity ratios, L/D exhibits the typical slow deformation followed by the asymptotical increase at a certain critical velocity gradient value. Such critical value and therefore the critical shear rate for breakup (the last data point) is significantly lower than that of the corresponding clean drops.

Table 2
Interfacial tension of various PDMS drops in PIB920 matrix at 25 °C.

Blend	Interfacial tension (clean) (mN/m)	Interfacial tension (after compatibilization) (mN/m)	
		Taylor's equation	Second order method (Hu) [35]
PIB920–PDMS0.1	2.176	0.55	0.60
PIB920–PDMS1	2.530	0.196	0.21
PIB920–PDMS10	2.445	0.15	0.17
PIB920–PDMS30	2.405	0.11	0.13
PIB920–PDMS60	2.442	0.26	0.27

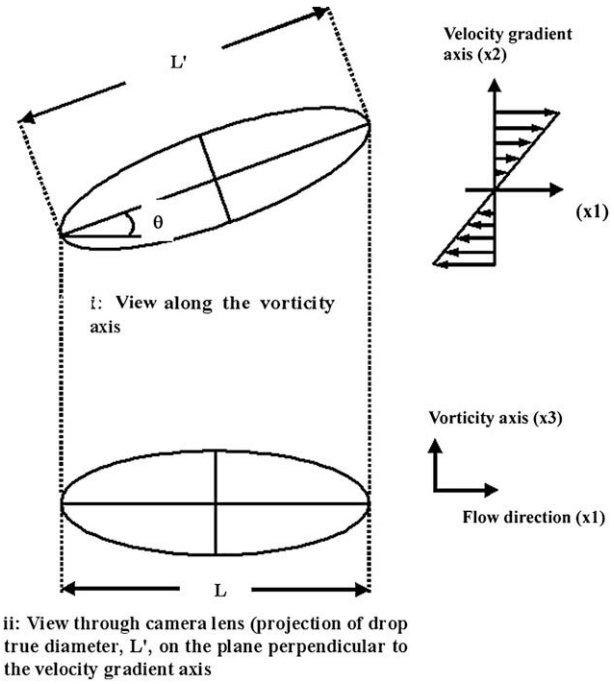

Fig. 3. Two views of the shearing drop: i) along the vorticity direction and ii) along the camera lens.

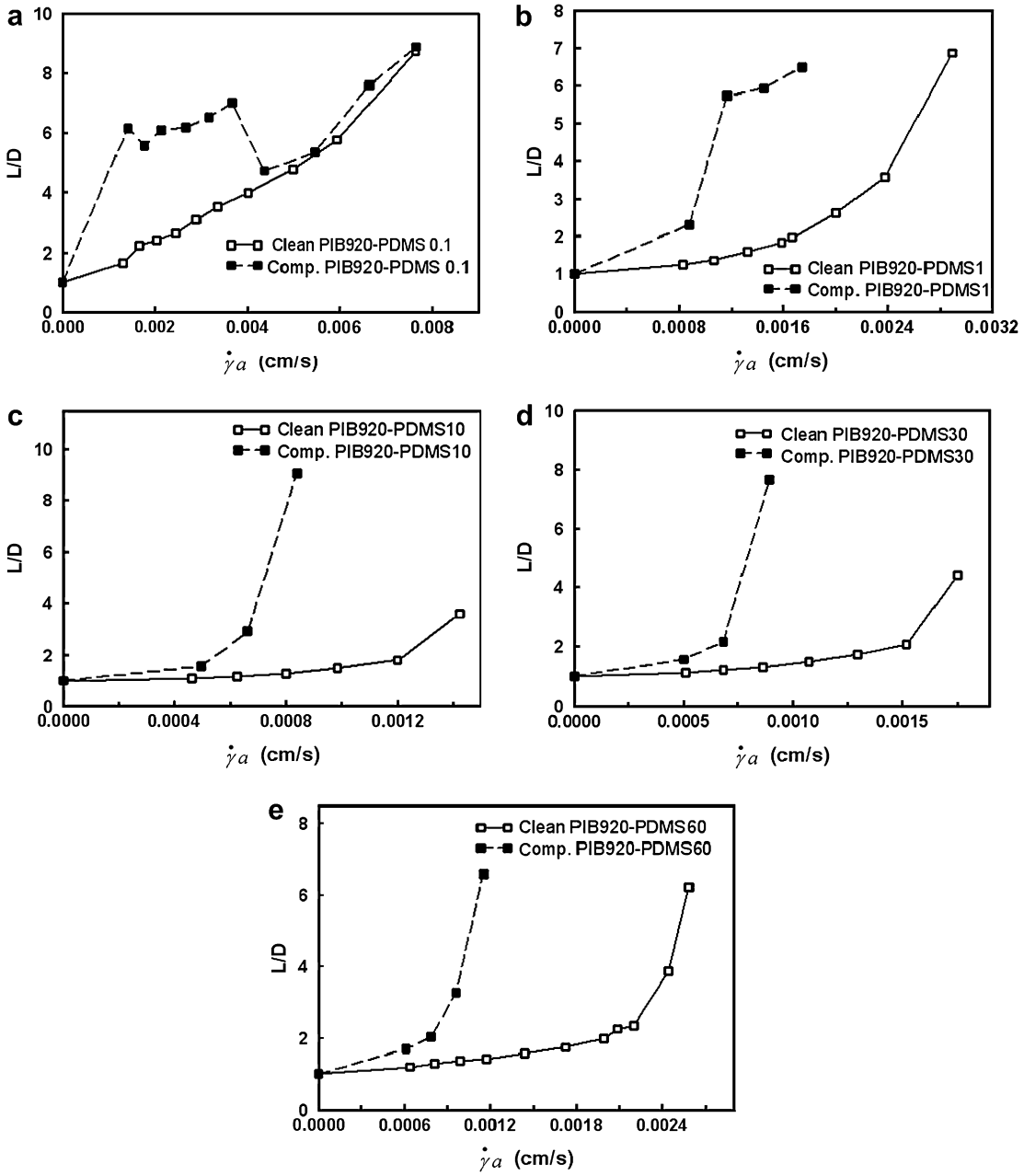

Fig. 4. (a) L/D vs. velocity gradient across the drop ($\dot{\gamma}a$) for PIB920/PDMS0.1 system ($p = 0.0039$, clean and compatibilized). (b) L/D vs. velocity gradient across the drop ($\dot{\gamma}a$) for PIB920/PDMS1 system ($p = 0.036$, clean and compatibilized). (c) L/D vs. velocity gradient across the drop ($\dot{\gamma}a$) for PIB920/PDMS10 system ($p = 0.41$, clean and compatibilized). (d) L/D vs. velocity gradient across the drop ($\dot{\gamma}a$) for PIB920/PDMS30 system ($p = 1.13$, clean and compatibilized). (e) L/D vs. velocity gradient across the drop ($\dot{\gamma}a$) for PIB920/PDMS60 system ($p = 2.317$, clean and compatibilized).

Typical variation of L/D as a function of time for various shear rates is shown in Fig. 5 for the highest viscosity ratio, $p = 2.317$. The curves for the other viscosity ratios are available but are not shown here for brevity reasons. The data corresponding to the various shear rates are reported on the same figure and are shown with different symbols. In each deformation state, the drop gets larger L/D comparing to the previous period due to the increase in shear rate. As the drop approaches the unsteady state regime, it presents unbounded deformation and a higher slope than the steady part. The unsteady state is reached earlier for compatibilized drop with much higher deformation.

Table 3 summarizes the critical velocity gradient and L/D ratios observed at breakup for the different viscosity ratios. L/D as a function of viscosity ratio for the clean drops follows the classical trend reported by Stone and Leal [4], but in the compatibilized case, a maximum is observed at a viscosity ratio that lies between 0.41 and 1.1. The lowest viscosity drop exhibits the strongest resistance to flow. Both for compatibilized and non-compatibilized cases, the critical velocity gradient passes through a minimum at a viscosity ratio that lies between 0.41 and 1.1. Except for the two lowest viscosity PDMS ($p = 0.0039$, $p = 0.036$ and due to tip-streaming), the reached L/D before breakup for other compatibilized drops is quite larger than L/D for the clean drops' counterparts. Therefore, the compatibilizer addition results in a decrease in the shear rate required to reach the critical L/D ratio for breakup and in an increase in the value of such critical L/D. These two effects can be assigned to the interfacial reduction combined with the absence of Marangoni stresses.

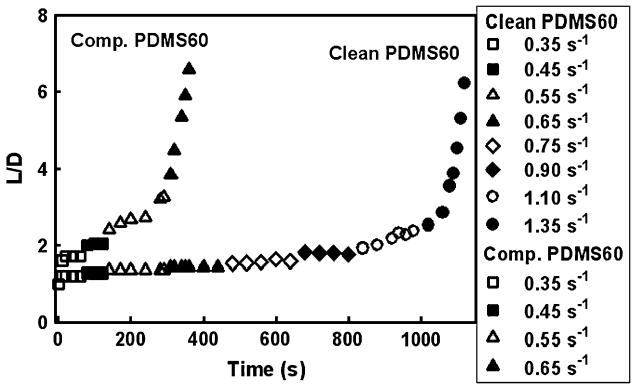

Fig. 5. Time evolution of L/D for PIB920/PDMS60 system ($p = 2.317$, clean and compatibilized).

A lower interfacial tension provides less resistance to deformation and therefore results in faster and higher amplitude of drop deformation in the low shear rate range. On the other hand, the effect of the interfacial tension lowering is to decrease the driving force for interfacial instabilities that induce breakup of the elongated drops. Therefore, highly elongated compatibilized drops are more stable than the clean drops, resulting in higher ultimate L/D ratios prior to breakup.

3.2. Visualization of drop deformation and breakup

3.2.1. Clean PDMS drop

Images of deforming PDMS drops at various shear rates and time intervals are presented in Fig. 6a–e. In each figure, distinction is made regarding the steady and the transient regimes. The scale bar given on the image for the undeformed initial drop represents 20 μm. Regardless of the viscosity ratio, the clean PDMS drops are deformed from their initial spherical shape into an ellipsoid in early stages followed by elongation into a long thread that eventually forms a waist prior burst. Except for the drop with the lowest viscosity ratio, $p = 0.0039$, the deformation and breakup processes are symmetric with the deformation axis and the drops show rounded ends until breakup. For the lowest viscosity drops, a completely different behavior is observed; the drop exhibits highly deformed shape up to high shear rates without thinning in the waist and its ends present a cusp-like shape. The tip-streaming, which is usually expected for low viscosity ratio systems was not observed in our case. The presence of tip-streaming depends crucially on the type of the drop liquid provided that the viscosity ratio is much smaller than unity as reported by De Bruijn [13]. De Bruijn did not observe tip-streaming for ester drops in silicone oil having viscosity ratios between 0.1 and 2×10^{-4}. The tip-streaming was only observed for standard silicon oil having a viscosity of 5×10^{-3} Pa s. The absence of such tip-streaming may also be due to the relatively small shear rate increments used in our experiments. In fact, Torza et al. [38] have shown that tip-streaming is promoted by abrupt changes in shear rates.

Table 3
Breakup data for clean and compatibilized drops with various viscosity ratios.

Viscosity ratio	Critical velocity gradient across the clean drop, $\dot{\gamma}a$ (cm/s)	Critical L/D (clean)	Critical velocity gradient across the compatibilized drop, $\dot{\gamma}a$ (cm/s)	Critical L/D (compatibilized)
0.0039	0.0076	8.73[a]	0.0076	8.87[a]
0.036	0.0029	6.88	0.00174	6.5
0.41	0.0014	3.59	0.00084	9.07
1.13	0.0018	4.42	0.00089	7.67
2.317	0.0026	6.22	0.0012	6.59

[a] This corresponds to the maximum deformation that could be captured in the camera view field and does not correspond necessarily to the deformation before breakup.

3.2.2. Compatibilized PDMS drop

Fig. 7a–e presents image series for the PDMS drops modified with 2 wt% PIB–PDMS copolymer. In the early deformation stages, the compatibilized drops deform in a similar manner as for their clean counterparts. However, the addition of the copolymer dramatically changes the end of the deformation process and the mechanism of breakup. Contrary to the clean drops, very little or no sign of symmetric necking and thinning in the drop waist is observed.

For the lower viscosity cases, $p = 0.036$ and $p = 0.0039$, the drop tips first become sharp and then stretch out (tip-stretching) even at relatively low shear rates generating a string of small daughter droplets (tip-streaming). The diameter of the stretching tips as well as that of the tip-streamed drops for $p = 0.0039$ is much smaller than those of $p = 0.036$. For the lowest viscosity drop, no tip-streaming could be observed at shear rates larger than 1.4 s^{-1}. The shape of the mother drop remains as well stable during tip-streaming with the shear rate and it later cleaves into three smaller parts.

For the intermediate viscosity ratios, $p = 1.13$ and $p = 0.41$, asymmetric drop deformation is observed. Interestingly, the drop with $p = 0.41$ takes a slender shape during unsteady deformation accompanied with short periods of tip-streaming. As the shear rate is increased, the drop further deforms up to a point where the ends are detached forming droplets having the same diameter as the main cylindrical mother drop (end-splitting).

The drop with the highest viscosity ratio, $p = 2.317$, is first distorted into an ellipsoidal shape before showing asymmetrical deformation upon increase in shear rate and then end-split at the critical shear rate of breakup. Similar results on the drop deformation were reported by Milliken et al. [26] who numerically examined the effect of dilute, insoluble surfactant on the transient motion of viscous drop in extensional flow. Their results showed that for the compatibilized drop with convective dominated regime, the drop deforms to a slender body shape before undergoing surface instabilities and then breakup process. In fact, diffusivity of our block copolymer with various molecular weights at the interface is of order of 10^{-13}–10^{-16} cm^2/s [24]. Using Eq. (4), along with the values of the drop radius and the applied shear rate, the corresponding Peclet number for the PIB920/PDMS system varies between 4.1×10^7 and 1.0×10^7 (4.1×10^7 for the lowest viscosity drop and 1.0×10^7 for the highest one). Such large values of the Peclet number result in a strong surface convective regime that discards any possibility of surface copolymer dilution.

3.3. Capillary number

Our experimental data for clean drops were fitted with the following empirical equation:

$$\log Ca_{crit} = -0.90 + 0.175(\log p)^2 + 0.0157(\log p)^3 - \frac{0.095}{\log p - \log 5} \quad (13)$$

The critical capillary numbers calculated from breakup data using Eq. (2) are shown in Fig. 8. For comparison purposes, the values obtained using the empirical equations (3) and (13), and also using Maffettone and Minale (MM) model [39] and Eq. (6) are also presented on the same figure. The MM model can only predict the

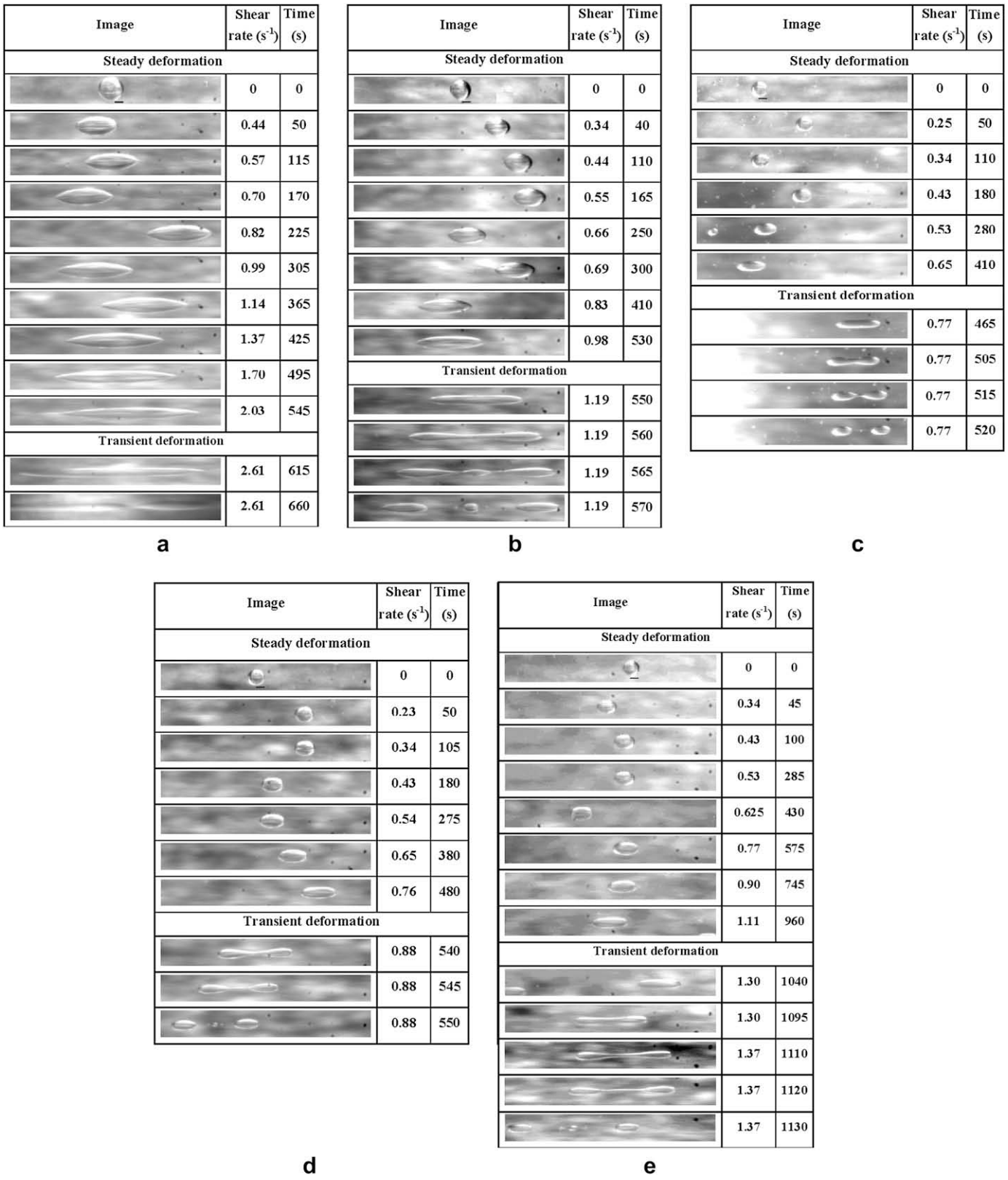

Fig. 6. Shape evolution of clean PDMS drop in PIB920 matrix; (a) $p = 0.0039$, (b) $p = 0.036$, (c) $p = 0.41$, (d) $p = 1.13$, (e) $p = 2.317$.

Ca_{crit} for the first three viscosity ratios. It is unable to predict the two largest ones.

The experimental data for the critical capillary number of clean drops follow the same trend as the experimental results of Grace [12] fitted by Eq. (3), with a minimum in Ca_{crit} for p lying between 0.41 and 1.1. Despite the similarities in the general trend, our results for $Ca_{crit} = f(p)$ are smaller than the ones reported by Grace for all viscosity ratios. Therefore, there are two possibilities: the first one

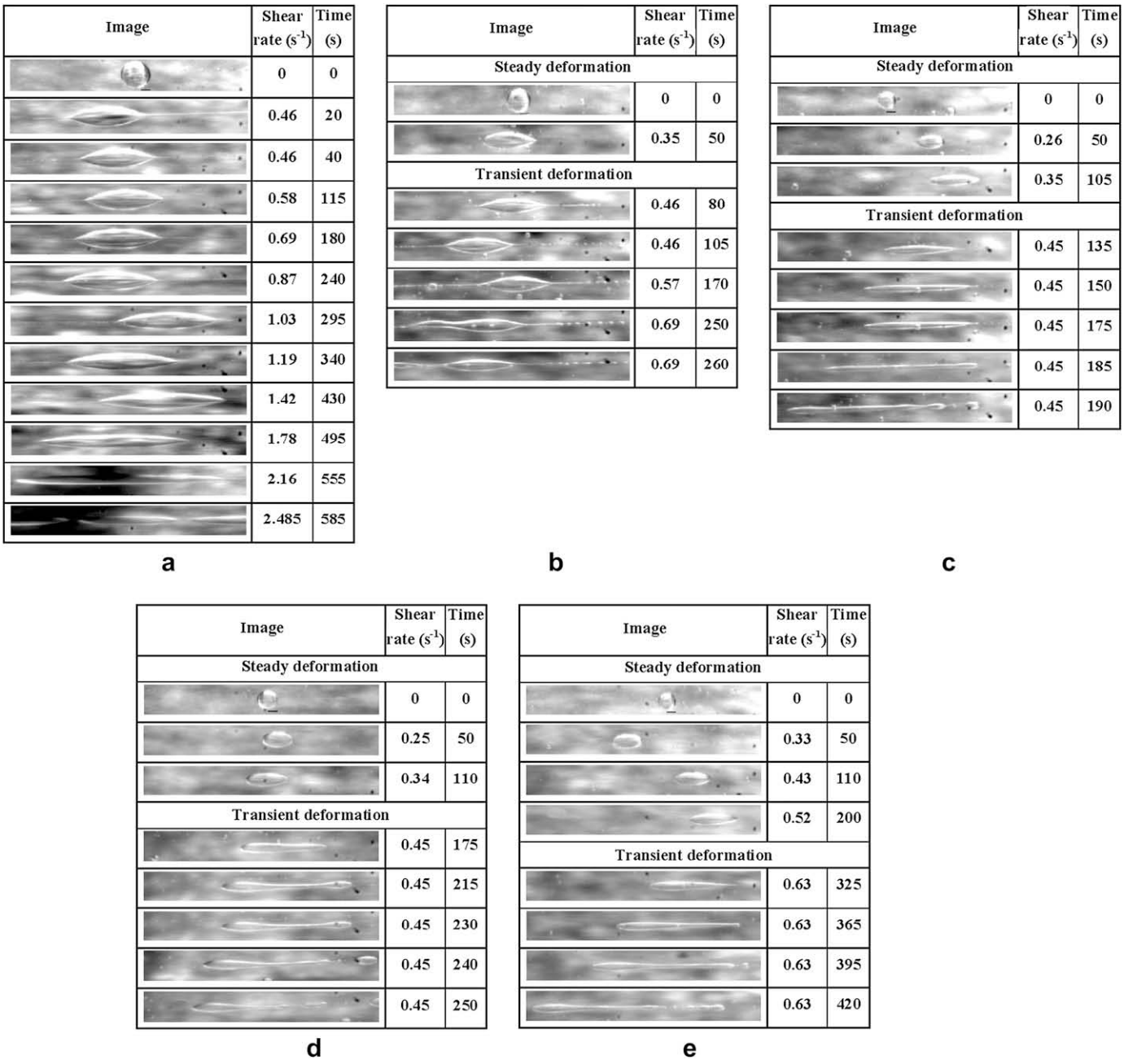

Fig. 7. Shape evolution of compatibilized PDMS drop in PIB920 matrix; (a) $p = 0.0039$, (b) $p = 0.036$, (c) $p = 0.41$, (d) $p = 1.13$, (e) $p = 2.317$.

is that the $Ca_{crit} = f(p)$ values of Grace are more accurate than ours. In this case, what matters in our experiments is only the relative difference between data for non-compatibilized case with those of the compatibilized one. In other words, if our device underestimates the shear rate, such underestimation would be normally the same for uncompatibilized and compatibilized cases, which does not influence the relative difference between the values of $Ca_{crit} = f(p)$ between uncompatibilized and compatibilized cases. This means that if we shift our curve for uncompatibilized case to match the Grace curve, the same shift should be applied to the compatibilized case, such that the same difference is obtained before the shifting operation.

The second possibility is that our home-made and patented device, which is made with more precise tools, gives more accurate results for both the imposed shear rate and for the imaging and the data acquisition than the Grace visualization device. In fact, the accuracy of setup was verified by comparing various rheological material functions measured on various polymeric systems with the results obtained using various constant-strain and constant-stress rheometers available in our laboratory (this issue is out of the scope of the present paper). Second, the literature reports some few studies about the reconstruction of the Grace curve ($Ca_{crit} = f(p)$) and in all cases, the reported results are either larger or lower than the Grace curve. In fact, the curve reported by Bentley and Leal [5] is slightly lower than the Grace curve. The results of Karam and Bellinger [40] show also a big difference comparing to the Grace data. The curve reported by Torza et al. [38] is located well below the Grace curve, while that reported by Stroeve et al. [41] is well above. Grace did a great job of monk, but the apparatus he had at his disposal was less precise in terms of both the imposed shear rates and in the image acquisition and data processing.

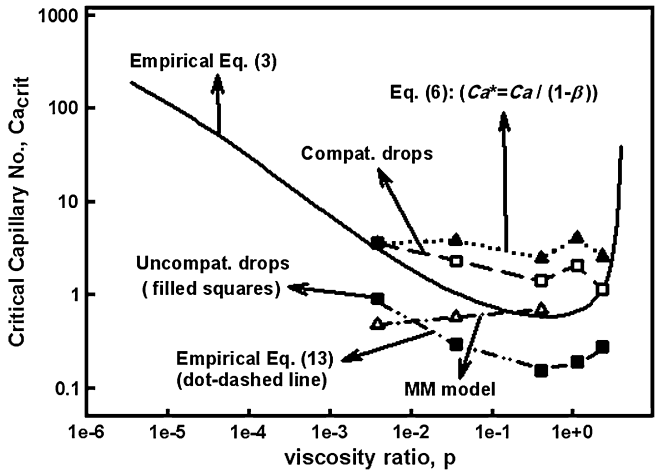

Fig. 8. Evolution of the critical capillary number for clean and compatibilized drops. The curve with the full line corresponds to the Grace experimental data fitted with Eq. (3).

The critical capillary number for the compatibilized drops is approximately one order of magnitude higher than that of the clean system. However, the drops with the highest and lowest viscosity present a lesser increase in the ratio of $(Ca_{compat}/Ca_{clean})_{crit}$. Velankar et al. [18] observed that for a compatibilized blend of PIB in PDMS having viscosity ratio $p \sim 1$, the steady shear capillary number is higher than the Ca_{crit} for the uncompatibilized drops. Contrary to the clean system that exhibits a minimum in Ca_{crit} for p between 0.41 and 1.1, the Ca_{crit} for the compatibilized drops does not follow any specific trend. This is directly related to difficulty to assess accurately the shear rate of breakup due to non-uniform deformation and breakup in copolymer modified drops. Such a behavior is related to non-uniform distribution of copolymer molecules along the surface of the deforming drop.

4. Concluding remarks

In this study, the effect of a PDMS–PIB block copolymer on the deformation and breakup behavior of Newtonian PDMS drops in a Newtonian PIB matrix has been examined using a home-made visualization Couette flow cell connected to a rheometer. The addition of the copolymer to the drop phase reduced the interfacial tension between PDMS and PIB by one order of magnitude. This led to a decrease in the critical shear rates required to breakup the drop. However, in the compatibilized case, the critical capillary number, which scales with the critical shear rate to interfacial tension coefficient, increased since in the presence of the block copolymer the interfacial tension dropped more than the critical shear rate.

Clean PDMS drops deformed symmetrically and formed a waist prior to breakup into an odd number of smaller droplets. By contrast, the compatibilized drops deformed asymmetrically, sharpened at the ends and finally went through tip-dropping or end-splitting. Deformation of the lower viscosity ratio drops was accompanied by tip-stretching and tip-streaming. Compatibilization of the lowest viscosity ratio drop, however, did not alter its breakup shear rate at all.

Finally, the experimental data obtained with a more accurate visualization device allowed us revising the classical Grace curve and providing a new one for blends compatibilized with an interfacial active agent with a given molecular weight.

Acknowledgement

This work was financially supported by the NSERC (Natural Sciences and Engineering Research Council of Canada) and Canada Research Chair on Polymer Physics and Nanomaterials and Steacie fellowship grants.

References

[1] Taylor GI. Proc R Soc London Ser A 1932;38:41–8.
[2] Taylor GI. Proc R Soc London Ser A 1934;146:501–23.
[3] Stone HA. Ann Rev Fluid Mech 1994;26:65–102.
[4] Stone HA, Leal LG. J Fluid Mech 1989;206:223–63.
[5] Bentley BJ, Leal LG. J Fluid Mech 1986;167:241–83.
[6] Grmela M, Bousmina M, Palierne JF. Rheol Acta 2001;40:560–9.
[7] Yu W, Bousmina M. J Rheol 2003;47:1011–39.
[8] Yu W, Zhou C, Bousmina M. J Rheol 2005;49:215–36.
[9] Yu W, Bousmina M, Zhou C. J Non-Newtonian Fluid Mech 2006;133:57–62.
[10] Deyrail Y, El Mesri Z, Huneault M, Zeghloul A, Bousmina M. J Rheol 2007; 51:781–97.
[11] Rallison JM. Ann Rev Fluid Mech 1984;16:45–66.
[12] Grace HP. Chem Eng Commun 1982;14:225–77.
[13] De Bruijn RA. PhD thesis, Eindhoven University of Technology, The Netherland; 1989.
[14] Rumscheidt FD, Mason SG. J Colloid Sci 1961;16:238–61.
[15] Yamane H, Takahashi M, Hayashi R, Okamoto K, Kashihara H, Masuda T. J Rheol 1998;42:567–80.
[16] Pesneau I, Ait Kadi A, Bousmina M, Cassagnau PH, Michel A. Polym Eng Sci 2002; 42:1990–2004.
[17] Hu YT, Pin DJ, Leal LG. Phys Fluids 2000;12(3):484–9.
[18] Velankar S, Van Puyvelde P, Mewis J, Moldenaers P. J Rheol 2001;45:1007–19.
[19] Van Puyvelde P, Velankar S, Mewis J, Moldenaers P. Curr Opin Colloid Interface Sci 2001;6:457–63.
[20] Van Puyvelde P, Velankar S, Mewis J, Moldenaers P. Polym Eng Sci 2002;42:1956–64.
[21] Velankar S, Van Puyvelde P, Mewis J, Moldenaers P. J Rheol 2004;48:725–44.
[22] Stone HA, Leal LG. J Fluid Mech 1990;220:161–86.
[23] Pawar Y, Stebe KJ. Phys Fluids 1996;8:1738–51.
[24] Mechbal N, Bousmina M. Macromolecules 2007;40:967–75.
[25] Eggleton CD, Pawar YP, Stebe KJ. J Fluid Mech 1999;385:79–99.
[26] Milliken WJ, Stone HA, Leal LG. Phys Fluids A 1993;5:69–79.
[27] Mark JE. Physical properties of polymers handbook. New York: AIP Press; 1996.
[28] Bousmina M, Mechbal N, Gagne S. US Patent 2007, WO/033479.
[29] Xing P, Bousmina M, Rodrigue D, Kamal MR. Macromolecules 2000;33: 8020–33.
[30] Ziegler VE, Wolf BA. Langmuir 2004;20:8688–92.
[31] Shi T, Ziegler VE, Welge IC, An L, Wolf BA. Macromolecules 2004;37:1591–9.
[32] Guido S, Simeone M, Villone M. Rheol Acta 1999;38:287–96.
[33] Nam KH, Jo WH. Polymr 1995;36:3727–31.
[34] Velankar S, Zhou H, Jeon HK, Macosko CW. J Colloid Interface Sci 2004; 272:172–85.
[35] Hu YT. J Colloid Interface Sci 2008;319:287–94.
[36] Yu W, Bousmina M, Zhou C. Rheol Acta 2004;43:342–9.
[37] Almusallam AS, Larson RG, Solomon MJ. J Rheol 2000;44:1055–83.
[38] Torza S, Cox RG, Mason SG. J Colloid Interface Sci 1972;38:395–411.
[39] Maffettonne PL, Minale M. J Non-Newtonian Fluid Mech 1998;78:227–41.
[40] Karam HJ, Bellinger JC. Ind. Engng Chem Fund 1968;7:576–81.
[41] Stroeve P, Prabodh PV, Elias T, Ulbrecht JJ. Stability of double emulsion droplets in shear flow. In: 53rd annual meeting of the society of rheology. Louisville, Kentucky; 1981.